Effect of perpendicular magnetic field on chaos in a cavity heated from below

Rajendra Prasad[1] and A. K. Singh[2]

Abstact - This paper presents chaotic behavior due to a magnetic field applied perpendicular on a cavity heated from below using the theory of dynamical system. The solution to the non-linear problem is obtained by using a truncated Galerkin method to obtain a set of ordinary differential equation for the time evolution of the Galerkin amplitudes. The system of differential equations is solved by using the fourth-order Runge Kutta method. Below a certain critical value of the scaled Rayleigh number the unique motionless conduction solution is obtained. At slightly super-critical values of scaled Rayleigh number a pitchfork bifurcation occurs, leading to two different steady solutions. For highly supercritical scaled Rayleigh numbers transition to chaotic solutions occurs via a Hopf bifurcation. The chaotic behaviour can be obtained faster for decreasing Hartmann number as well as incrasing scaled Rayleigh number . Also variation in Nusselt number inreases with increasing scaled Rayleigh number and decreasing Hartmann number.

Keywords— Chaotic behaviour, Magnetic field , Lorenz equations.

1. NTRODUCTION

Chaos convection plays an important role in the laboratory, for example, chaos can be applied in the design of electrical circuits, lasers, and mechanical and magneto-mechanical devices as well as in understanding oscillatory chemical reactions and fluid dynamics, and in the nature, chaos theory also applies in dynamics of satellites in the solar system, time evolution of the magnetic field of celestial bodies, population growth in ecology and molecular vibration as well as in the weather and climate.

It is not often that it is possible to establish analytically the nature of chaotic solutions observed numerically in the partial differential equations. Rucklidge [1] showed how the PDEs for a two dimensional Boussinesq convection in a vertical magnetic field could be reduced for a particular range of parameters, first to a third order set of ordinary differential equations and then to a one dimensional map. The analysis of the map shows an abrupt transition from periodic to chaotic behaviour.

The problem of Rayleigh-Benard convection interacting with a magnetic field, which is called magnetoconvection, has been investigated by many authors Weiss [2], [3] first carried out numerical simulations of the partial differential equations for a two-dimensional Boussinesq magnetoconvection and showed that the magnetic flux was concentrated into sheets at the sides of the square cell, from which the motion was excluded. Weiss [3] also found a periodic behavior that did not settle down to regular oscillations after ten cycles in a certain range of parameters. Knobloch et al. [4]-[6] studied a fifth-order truncation of PDEs for magnetoconvection, which is a straightforward extension of the Lorenz model [7] and reported a bifurcation structure of that truncation model in acertain region of parameters. Rucklidge [8] derived a third-order set of ordinary differential equations that governed the behavior of PDEs near a co-dimension three bifurcation and found the first chaotic oscillations of the third-order system observed numerically in PDEs. Rucklidge et al. [9], [10] carried out numerical simulations of compressible three-dimensional magnetoconvection and showed complicated spatiotemporal behavior. Nonlinear modulational dynamics of travelling rolls in three-dimensional magnetoconvection was investigated near the onset of a Hopf bifurcation and criteria for the modulational instability of travelling rolls were obtained by means of the reductive perturbation method. Cox [11] and Matthews [12] found an excitation of large-scale modulation of amplitude of two-dimensional Boussinesq magnetoconvection which was closely related to the excitation of the convective-cell modes in drift wave turbulence.

The route to chaos in a fluid layer has been studied extensively since the work of Lorenz [7], who studied a two dimensional fluid cell heated from below and cooled from above (also known as the Raleigh-Benard problem) in order to model unpredicted behaviour in weather. Then he proposed the three-dimensional set of partial differential equation known as the model of convection and suggested that it is difficult to reach good accuracy in very long range forecasting because this model gives rise to chaotic behaviour (Chen and Price [13]).

Rucklidge [1], [9] studied chaos in magneto-convection and found that the chaotic behaviour governed by partial differential equation (PDEs) provides a more accurate solution

First Author, Rajendra Prasad[1] is working as a Research Fellow in the Department of Mathematics, Faculty of Science, Banaras Hindu University, Varanasi – 221005, India (corresponding author to provide mob. No. 09839086708; e-mail: rajendrabhu108@gmail.com).

Second Author, Ashok Kumar Singh[2] is working as a Professor in the Department of Mathematics, Faculty of Science, Banaras Hindu University,Varanasi – 221005, India (Second Author to provide mob. No. 09450530760; e-mail: ashok@bhu.ac.in).

than do ordinary differential equation (ODEs) which govern the Lorenz system. He reported that the transition from periodic orbits to chaotic Lorenz attractor predicted by ODEs is also recovered in PDEs. Bekki and Moriguchi [14] investigated chaos in Boussinesq magneto-convection with stress-free boundary conditions. Their results showed that the long-term behavior of magneto-convection exhibits spatially coherent and temporally chaotic rolls, in marked contrast to the long-term behavior of highly turbulent fluids. Garandet et al. [15] claimed that the fluid in this enclosure experiences the mechanism of buoyancy, due to fluid density changes caused by temperature variations resulting from heat transfer and the interaction of the magnetic field with the convective motion. Garandet et al. [15] assumed the magnetic Reynolds number to be small; therefore the induced magnetic field can be assumed to be negligible i.e. it has virtually no effect on the applied magnetic field.

The objective of this paper is to demonstrate the possible convection regimes at supercritical values of Rayleigh number and also the effect of the perpendicular magnetic field on transition to chaos in a cavity heated from below. The solution to the non-linear problem is obtained by using a truncated Galerkin method to obtain a set of ordinary differential equation for the time evolution of the Galerkin amplitudes. The system of differential equations is solved by using the fourth-order Runge Kutta method.

2 Problem Formulation

2.1 Basic Equations

Here, the unsteady free convective flow of a viscous incompressible and electrically conducting fluid in a cavity of length L and width H is considered. The x'-axis is taken along the bottom and y'-axis transverse to it having origin at the lower end of the left wall as shown in Fig.1. A constant magnetic field B_0 is applied perpendicular to the cavity along z'-axis.

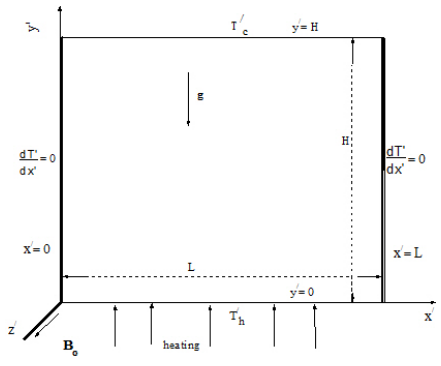

Fig. 1: Physical model and coordinate system

The flow is assumed to be at small magnetic Reynolds number and hence the induced magnetic field can be neglected. The left and right walls are thermally insulated while the horizontal top and bottom walls of the cavity are maintained at isothermal but different temperature T_c' and T_h', respectively. The viscous and Ohmic dissipation terms have been neglected. By using the Boussinesq approximation, the governing equations - continuity, momentum and thermal energy in two dimensional form, can be written as:

$$\frac{\partial u'}{\partial x'}+\frac{\partial v'}{\partial y'}=0, \tag{1}$$

$$\frac{\partial u'}{\partial t'}+u'\frac{\partial u'}{\partial x'}+v'\frac{\partial u'}{\partial y'}=-\frac{1}{\rho_0}\frac{\partial p'}{\partial x'}+\nu\nabla^2 u'-\frac{\sigma B_0^2}{\rho_0}u', \tag{2}$$

$$\frac{\partial v'}{\partial t'}+u'\frac{\partial v'}{\partial x'}+v'\frac{\partial v'}{\partial y'}=-\frac{1}{\rho_0}\frac{\partial p'}{\partial y'}+\nu\nabla^2 v'-g[1-\beta(T'-T_c')]-\frac{\sigma B_0^2}{\rho_0}v', \tag{3}$$

$$\frac{\partial T'}{\partial t'}+u'\frac{\partial T'}{\partial x'}+v'\frac{\partial T'}{\partial y'}=\alpha_T\nabla^2 T'. \tag{4}$$

where u' and v' are the velocity components in the $x'-axis$ and $y'-axis$ directions, respectively, p' the pressure, T' the temperature, ν the kinematic viscosity, α_T the thermal diffusivity, σ the electrical conductivity and β is the coefficient of the volumetric extension.

For the flow model considered, the boundary conditions for the velocity and temperature fields are given by

$$u'=v'=0 \quad at \quad x'=0,L \quad and \quad at \quad y'=0,H, \tag{5}$$

$$T'=T_h' \quad at \quad y'=0 \quad and \quad T'=T_c' \quad at \quad y'=H, \tag{6}$$

$$\frac{\partial T'}{\partial x'}=0 \quad at \quad x'=0 \quad and \quad at \quad x'=L. \tag{7}$$

Now introducing the stream function defined as

$$(u',v')=\left(\frac{\partial \psi'}{\partial y'},-\frac{\partial \psi'}{\partial x'}\right), \tag{8}$$

and the non-dimensional quantities

$$(x,y)=(x',y'),\ (u,v)=(u',v')L/\alpha;\ T=(T'-T_c')/(T_h'-T_c')$$

$$and\ \ \psi=\psi'/\alpha_T,\ t=t'\alpha_T/L^2,\ \nabla=\nabla' L^2; \tag{9}$$

the Eq. (8) takes the non-dimensional form as

$$(u,v)=\left(\frac{\partial \psi}{\partial y},-\frac{\partial \psi}{\partial x}\right), \tag{10}$$

while the Eqs. (2) - (4) can be expressed as follows:

$$\frac{\partial(\nabla^2\psi)}{\partial t}-\frac{\partial(\psi,\nabla^2\psi)}{\partial(x,y)}=Pr\nabla^2(\nabla^2\psi)-RaPr\frac{\partial T}{\partial x}-Ha^2Pr\nabla^2\psi, \tag{11}$$

$$\frac{\partial T}{\partial t}-\frac{\partial(\psi,T)}{\partial(x,y)}=\nabla^2 T. \quad (12)$$

In Eqs. (11) and (12), we have introduced a number of well-known non-dimensional parameters, namely, the Rayleigh number (Ra), Prandtl number (Pr) and Hartmann number (Ha) and these are defined as follows:

$$Ra=g\beta(T_h^{'}-T_c^{'})L^3/\nu\alpha_T,\ Pr=\nu/\alpha_T,\ Ha^2=\sigma B_0^2L^2/\rho\nu. \quad (13)$$

The set of boundary conditions Eqs. (5) - (7) can be shown to transform in non-dimensional form are as follows

$$\psi=0 \quad at \quad x=0, Ar \quad and \quad at \quad y=0,1; \quad (14)$$

$$T=1-y \quad at \quad y=0 \quad and \quad at \quad y=1; \quad (15)$$

$$\frac{\partial T}{\partial x}=0 \quad at \quad x=0 \quad and \quad at \quad x=Ar; \quad (16)$$

where the aspect ratio Ar is defined as, $Ar=L/H$.

3. Truncated Galerkin expansion

To obtain the solution of the non-linear system of the partial differential Eqs.(11) and (12), we represent the stream function and temperature in the form (Lorentz [7])

$$\psi=A_1\sin(\frac{\pi x}{Ar})\sin(\pi y), \quad (17)$$

$$T=1-y+B_1\cos(\frac{\pi x}{Ar})\sin(\pi y)+B_2\sin(2\pi y). \quad (18)$$

This representation is equivalent to the Galerkin expansion of the solution in both the $x-$ and $y-$ directions. Substituting Eqs. (17) and (18) in Eqs. (11) and (12) and then multiplying the equations by the corresponding orthogonal characteristic functions of Eqs. (17) and (18) and finally integrating them over the domain $[0,Ar]\times[0,1]$, we obtain a set of three ordinary differential equations for the time evolution of the amplitudes as

$$\frac{dA_1(\tau)}{d\tau}=-\frac{Pr\gamma}{\pi^2}[\frac{\pi^2}{\gamma}A_1(\tau)+Ha^2A_1(\tau)+\frac{Ra_T}{\pi\theta}B_1(\tau)] \quad (19)$$

$$\frac{dB_1(\tau)}{d\tau}=-\frac{1}{\pi\theta}A_1(\tau)-\frac{1}{\theta}A_1(\tau)B_2(\tau)-B_1(\tau), \quad (20)$$

$$\frac{dB_2(\tau)}{d\tau}=-4\gamma B_2(\tau)+\frac{1}{2\theta}A_1(\tau)B_1(\tau). \quad (21)$$

In Eqs. (19) - (21), the time is rescaled and some additional notations have been used and they are as follows:

$$\tau=\frac{\pi^2 t}{\gamma},\quad \gamma=\frac{Ar^2}{Ar^2+1},\quad and \quad R=\frac{Ra}{\pi^2\theta^2}. \quad (22)$$

Rescaling of the amplitudes in the form of

$$X(\tau)=-\frac{A_1(\tau)}{2\theta\sqrt{2\gamma(R-1)}},\ Y(\tau)=\frac{\pi RB_1(\tau)}{2\sqrt{2\gamma(R-1)}} \quad and \quad Z(\tau)=-\frac{\pi RB_2(\tau)}{R-1}, \quad (23)$$

in Eqs. (19) – (21), we get the following set of simultaneous differential equations:

$$\frac{dX}{d\tau}=\alpha[Y-(C+Ha^2)X], \quad (24)$$

$$\frac{dY}{d\tau}=RX-Y-(R-1)XZ, \quad (25)$$

$$\frac{dZ}{d\tau}=4\gamma(XY-Z). \quad (26)$$

where

$$\alpha=\frac{Pr\gamma}{\pi^2},\quad C=\pi^2/\gamma. \quad (27)$$

Eqs. (24) – (26) are like the Lorenz equations [7], with different coefficients.

4 Stability Analyses

The non-linear dynamics of system (24) – (26) has been analyzed and solved for $\alpha=0.1$ and $\gamma=0.1$ corresponding to a convection. We consider in this section the thermal instability of buoyancy-driven flow of a viscous incompressible and electrically conducting fluid in a cavity. The fluid layer is subjected to a constant horizontal temperature gradient. Stability analysis of the stationary solutions was performed in order to determine the nature of dynamics about the fixed points.

4.1 Dissipation

The system given by Eqs. (24) – (26) is a dissipative because

$$\nabla.V=\frac{\partial\dot{X}}{\partial X}+\frac{\partial\dot{Y}}{\partial Y}+\frac{\partial\dot{Z}}{\partial Z}=-[\alpha(C+Ha^2)+1+4\gamma]<0. \quad (28)$$

Eq. (28) implies that, if the set of initial points in the phase space occupies the region $V(0)$ at time $t=0$,then after some time t, the end points of the trajectories will falling as $V(t)$ given by

$$V(t)=V(0)\exp[-\{\alpha(C+Ha^2)+1+4\gamma\}t]. \quad (29)$$

The above expression clearly shows that the volume of the system decreases monotonically with the time.

4.2 Equilibrium points

We can see that the dynamical system represented by Eqs. (24) – (26) has the general form $\dot{X}=f(X)$ and the equilibrium (fixed or stationary) points X_s are given by $f(X_s)=0$. The equilibrium points of the rescaled system are

$$(X_1, Y_1, Z_1) = (0,0,0), \tag{30}$$

$$X_2, X_3 = \pm\sqrt{\frac{R-(C+Ha^2)}{(R-1)(C+Ha^2)}}, \tag{31}$$

$$Y_2, Y_3 = \pm\sqrt{\frac{[R-(C+Ha^2)](C+Ha^2)}{R-1}}, \tag{32}$$

$$Z_2 = Z_3 = \frac{R-(C+Ha^2)}{R-1}, \tag{33}$$

corresponding to the convection solutions.

4.3 Stability of Equilibrium Points

By linearizing the system of Eqs. $(24)-(26)$, the Jacobian matrix is obtained as follows:

$$J = \begin{bmatrix} -\alpha(C+Ha^2) & \alpha & 0 \\ R-(R-1)Z & -1 & -(R-1)X \\ 4\gamma Y & 4\gamma X & -4\gamma. \end{bmatrix} \tag{34}$$

The characteristic values of the Jacobian matrix obtained by solving the zeros of the characteristic polynomial provide the stability conditions. A fixed point is stable if all the eigenvalues are negative (or in the case of complex eigenvalues, the real parts are negative). However, a fixed point is not stable when atleast one eigenvalues becomes positive (or in the case of complex eigenvalues,it has positive real part).

The stability of the fixed point corresponding to the motionless solution $X_1 = 0, Y_1 = 0, Z_1 = 0$ is controlled by the zeros of the following characteristic polynomial equation for the eigenvalues, $\lambda_i (i = 1,2,3)$:

$$(4\gamma+\lambda)[\alpha R-(1+\lambda)(\alpha C+\alpha Ha^2+\lambda)] = 0. \tag{35}$$

The eigenvalues are

$$\lambda_1 = -4\gamma, \tag{36}$$

$$\lambda_2, \lambda_3 = \frac{1}{2}[-\{\alpha(C+Ha^2)+1\} \pm \sqrt{\{\alpha(C+Ha^2)+1\}^2 - 4\alpha\{R-(C+Ha^2)\}}] \tag{37}$$

$$R_{c1} = R_{cr} = C + Ha^2, \quad or \quad Ra_{cr} = 4\pi^2(C+Ha^2) \tag{38}$$

The stability of the fixed points corresponding to the convection solution (X_2, Y_2, Z_2) and (X_3, Y_3, Z_3) is controlled by the following equation for the eigenvalues, $\lambda_i (i = 1,2,3)$:

$$\begin{aligned}&(C+Ha^2)\lambda^3 + (C+Ha^2)[\alpha(C+Ha^2) \\ &+ 4\gamma + 1]\lambda^2 + [4\gamma((C+Ha^2)^2 + R)]\lambda \\ &+ (C+Ha^2)[8\alpha\gamma(R-(C+Ha^2))] = 0.\end{aligned} \tag{39}$$

Eq. (40) yields three eigenvalues, all the roots are real and negative at slightly supercritical value of R and the convection fixed points are stable, that is simple nodes. These roots move on the real axis towards the origin as the value of R increases. These roots become equal when

$$R = \frac{\alpha(C+Ha^2)^2[\alpha(C+Ha^2)+4\gamma+3]}{\alpha(C+Ha^2)-4\gamma-1}. \tag{40}$$

Table 1: Values of R where λ_2, λ_3 become equal when the loss of stability occurred for the different values of Ha.

H	$R(\lambda_2 = \lambda_3)$	R (loss of stability occured)
10	198.69	3500
15	323.69	4000
20	498.69	4500
25	723.69	6300

In table 1., we have listed the values of R for different values of Ha. Here, we observe that on increasing Ha, the supercritical values of R also increase .

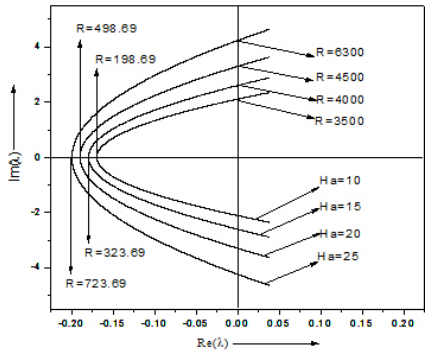

Fig. 2: Evolution of the complex eigenvalues with increasing Rayleigh number, for $Ha = 10,15,20,25.$

Fig. 2. shows that at $Ha = 10,15,20$ and 25, both roots λ_2, λ_3 are purely real, negative and equal. When we take the slightly supercritical value of R, the roots become complex conjugate with negative real part and further on increasing the value of R, they approach towards the origin on the real axis, the smallest between the two chasing the other one and reducing the distance between them. However, they have still negative real parts, therefore the convection fixed points are stable i.e spiral nodes. Corresponding to Hartmann Number $Ha = 10,15,20$ and 25 the roots become purely imaginary i.e their real parts becomes zero at $R = 3500,4000,4500$ and 6300. Again on increasing the value of R, both the imaginary and the real parts of these two complex conjugate

eigenvalues increase and on the complex plane, they cross the imaginary axis i.e their real part becomes positive and motion is unstable.

5 Heat Transport

In engineering point of view, one of the important characteristic of the flow is to see the import of physical parameters on the rate of heat transfer across the cavity, and this is estimated by computing the values of the Nusselt number, Nu. The local Nusselt number on the horizontal bottom of the cavity is defined by

$$Nu = \left(\frac{\partial T}{\partial y}\right)_{y=0} \tag{41}$$

The overall heat transfer rate across the cavity, expressed by the average Nusselt number at the horizontal bottom, is obtained as

$$Nu_{av}\,|_{y=0} = \frac{1}{A_r}\int_0^{A_r} Nu\,dx \tag{42}$$

Using Eqs. (18) and (41) in Eq. (42), we get

$$Nu_{av}\,|_{y=0} = \left(-1+\frac{2(1-R)}{R}Z\right) \tag{43}$$

Substituting the value of Z in Eq. (43), we can obtain the average Nusselt number at the horizontal bottom.

6 Result and Discussion

In order to see the dynamic behaviour of the system, we present some numerical simulations of the system of Eqs. $(24)-(26)$ for the time domain $0 \le t \le 80$. All the calculations are performed by using the Runge-Kutta method of fourth-order on double precision when the time step is 0.001, by fixing the values $\alpha = 0.1, \gamma = 0.1$ and taking the common initial conditions as $X(0) = 0.05,\ Y(0) = 0.5,\ Z(0) = 0.9$ in the neighbourhood of the positive convective fixed point. Here, we shall demonstrate different possible solutions and transition values of R and Ha for the fixed value of α and γ.

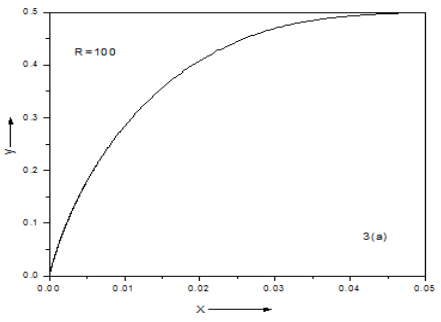

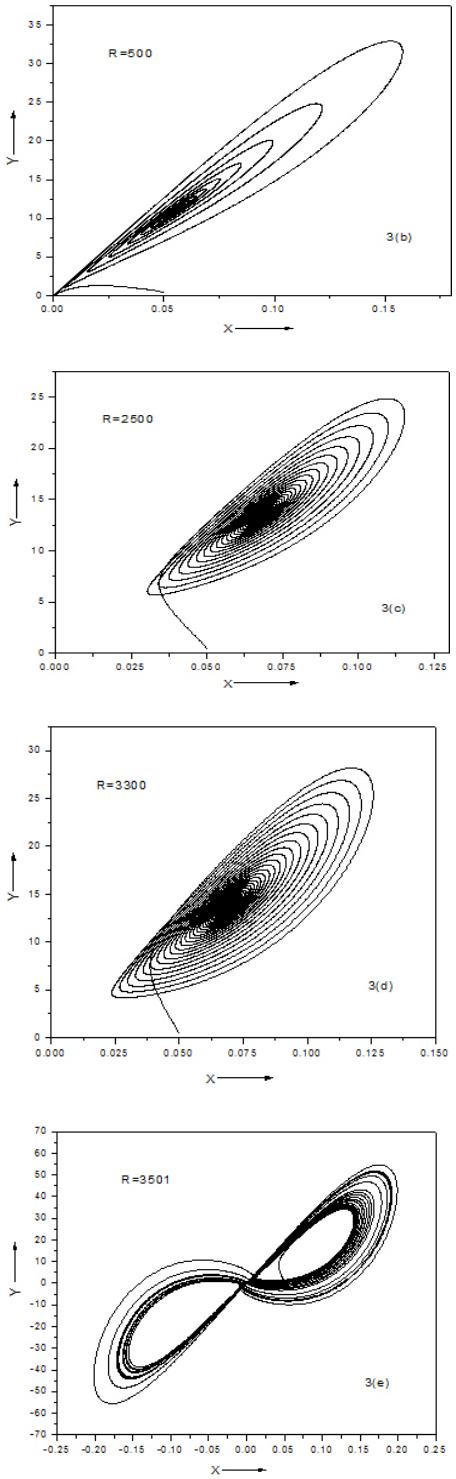

Fig. 3: Computational results for the evolution of trajectories over time in the state space for the increasing values of scaled Rayleigh number (R). the graphs represent the projection of the solution data points onto $X-Y$ plane for $Ha = 10.$

The evolution of trajectories over time in the state space for increasing values of scaled Rayleigh number is presented in Fig. 3, in terms of the projections of trajectories onto the $X-Y$ plane for $Ha = 10.$ From Fig. $3a$, it is evident that the trajectory is like a concave curve with respect to the x-axis and moving to the steady convection point starting from initial

point $(0.05,0.5,0.9)$ for $R = 100$ i.e. the convection solution is a stable simple node. The motionless solution losses its stability for a Rayleigh number slightly above $R_{c1} = 198.69$. In Fig. $3b$, For $R = 500$ the solutions shows that the trajectory is attracted to the convective fixed point via a spiral i.e. the fixed point is a stable spiral node, which predicated a transition of the two originally real roots to a pair of complex conjugate roots at a value of $R_{c1} = 198.69.$ Fig. $3c$ and $3d$ show that for higher values of R i.e. $R = 2500$ and $R = 3300$, the spiraling approach of the trajectories towards the fixed point becomes faster. For $R = 3501$, the real part of the of complex conjugate eigen-values becomes positive and hence the convective fixed points losses their stability and it can be seen in Fig. 3e in which the transition to chaotic solution occurs.

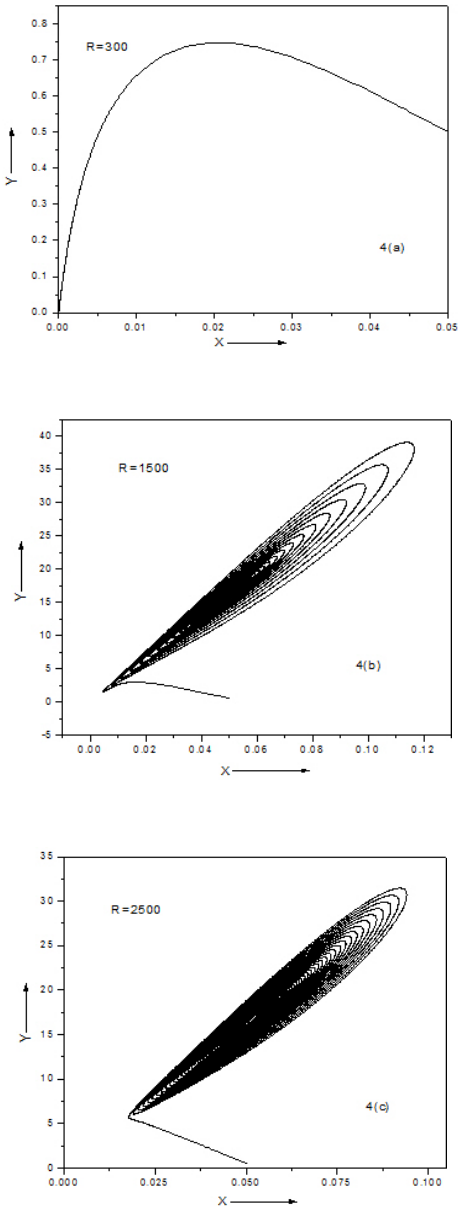

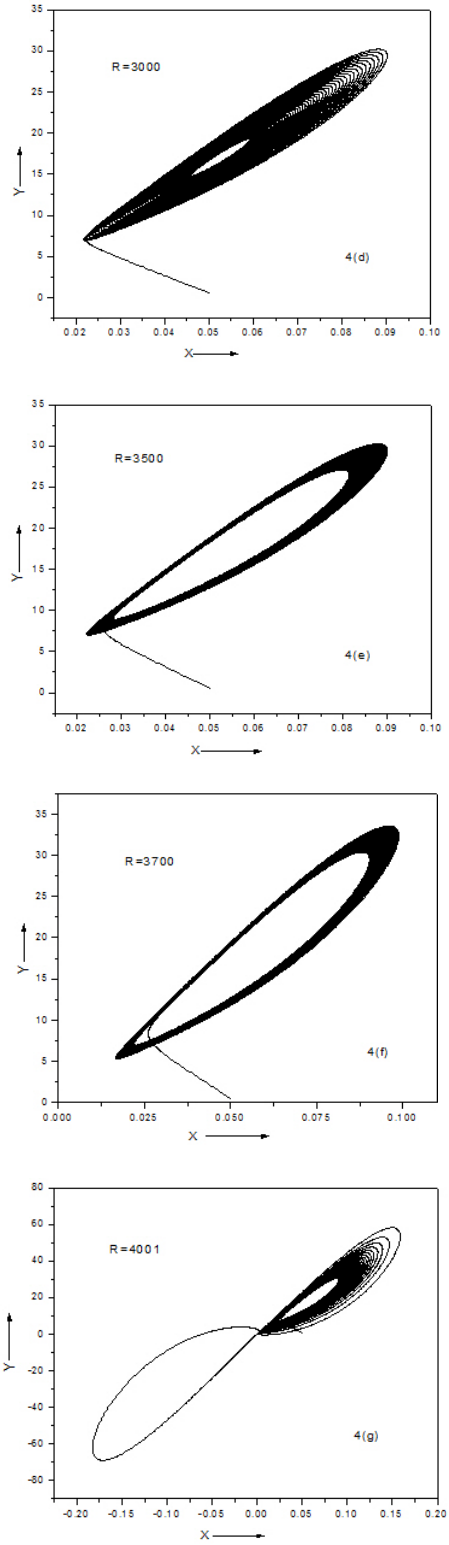

Fig. 4: Computational results for the evolution of trajectories over time in the state space for the increasing values of scaled Rayleigh number (R). the graphs represent the projection of the solution data points onto $X-Y$ plane for $Ha = 15$.

In Fig. 4, we have presented the evolution of trajectories over time in the state space for increasing values of the scaled Rayleigh number at $Ha = 15$ in terms of the projections of trajectories onto the $X-Y$ plane. It is evident from Fig. $4a$

that the trajectory is a concave curve with respect to the X-axis and moving to the steady convection point starting from initial point $(0.05,0.5,0.9)$ for $R = 300$ and thus, the convection solution is a stable simple node. In this case, the motionless solution losses its stability for the Rayleigh number slightly above $R_{c1} = 323.69$. Fig. $4b$ for $R = 1500$ shows that the trajectory is attracted to the convective fixed point in the form of a spiral. It shows that the fixed point is a stable spiral node. Further, from Figs. $4c$, $4d$ and $4e$ at $R = 2500,3000$ and 3500 respectively, we can see that the trajectories approach to the convective fixed point on a spiral and the closeness of spiraling near the fixed point increase on increasing the value of R i.e the stability of the convective fixed point losses by increasing the value of R. Fig. $4f$ clearly indicates that a limit cycle is created i.e. the solution is not heading any more towards the convective fixed point but rather fluctuates periodically around it. Fig. $4g$ at $R = 4001$ (when the real part of the pair of complex conjugate eigenvalues become positive) shows that the convective fixed points lose their stability i.e. chaotic solution occurs.

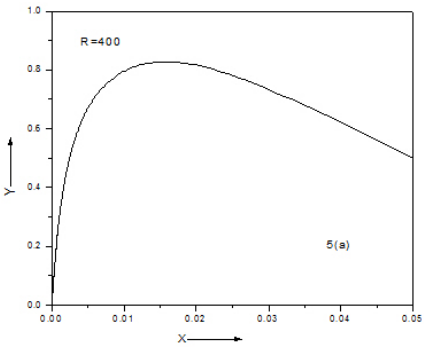

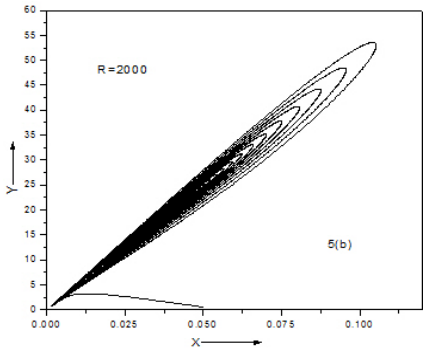

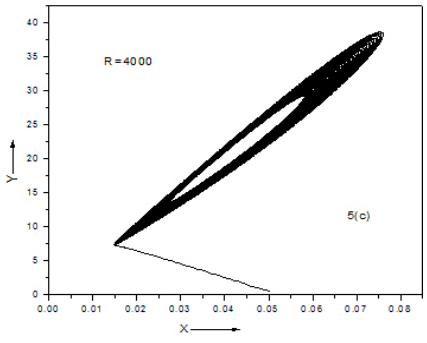

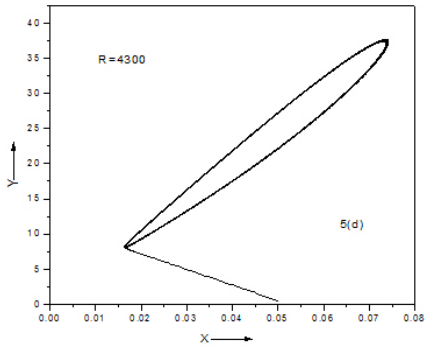

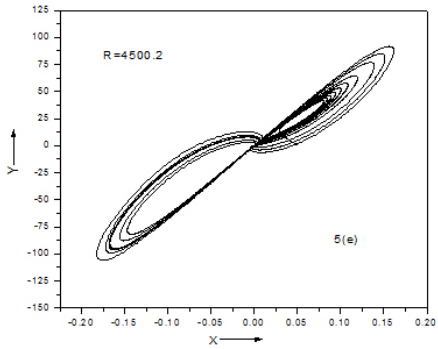

Fig. 5: Computational results for the evolution of trajectories over time in the state space for the increasing values of scaled Rayleigh number (R). the graphs represent the projection of the solution data points onto $X-Y$ plane for $Ha = 20$.

When $Ha = 20$, we found that at $R_{c1} = 498.69$, the motionless solution loses stability and the convection solution occurs. For $R = 4500.2$, the convection fixed points lose their stability and a chaotic solution takes over. The evolution of trajectories over time in the state space for increasing values of the scaled Rayleigh number is presented in Fig. 5 in terms of the projections of trajectories onto the $Y-X$ plane. From Fig. $5a$, it is evident that the trajectory is like a concave curve w.r.t the x axis and moving to the steady convection point starting from initial point $(0.05,0.5,0.9)$ for $R = 400$ i.e the convection solution is a stable simple node. The motionless solution losses its stability for a Rayleigh number slightly above $R_{c1} = 498.69$.

For $R = 2000$, Fig. $5b$ shows that the trajectory is attracted to the convective fixed point via a spiral i.e the fixed point is a stable spiral node, which predicated a transition of the two originally real roots to a pair of complex conjugate roots at a value of $R_{c1} = 498.69$.

At $R = 4000$ the spiraling approach increases towards the fixed point but closeness decrease than $R = 2000$ as shown in Figs. $5c$ and $5b$ respectively. At the value of $R = 4300$, we obtain a solitary limit cycle indicating the loss of stability of the convection fixed points (Fig. $5d$). We can observe in Fig. 5e that the transition to chaotic solution occurs at a critical value of $R = 4500.2$

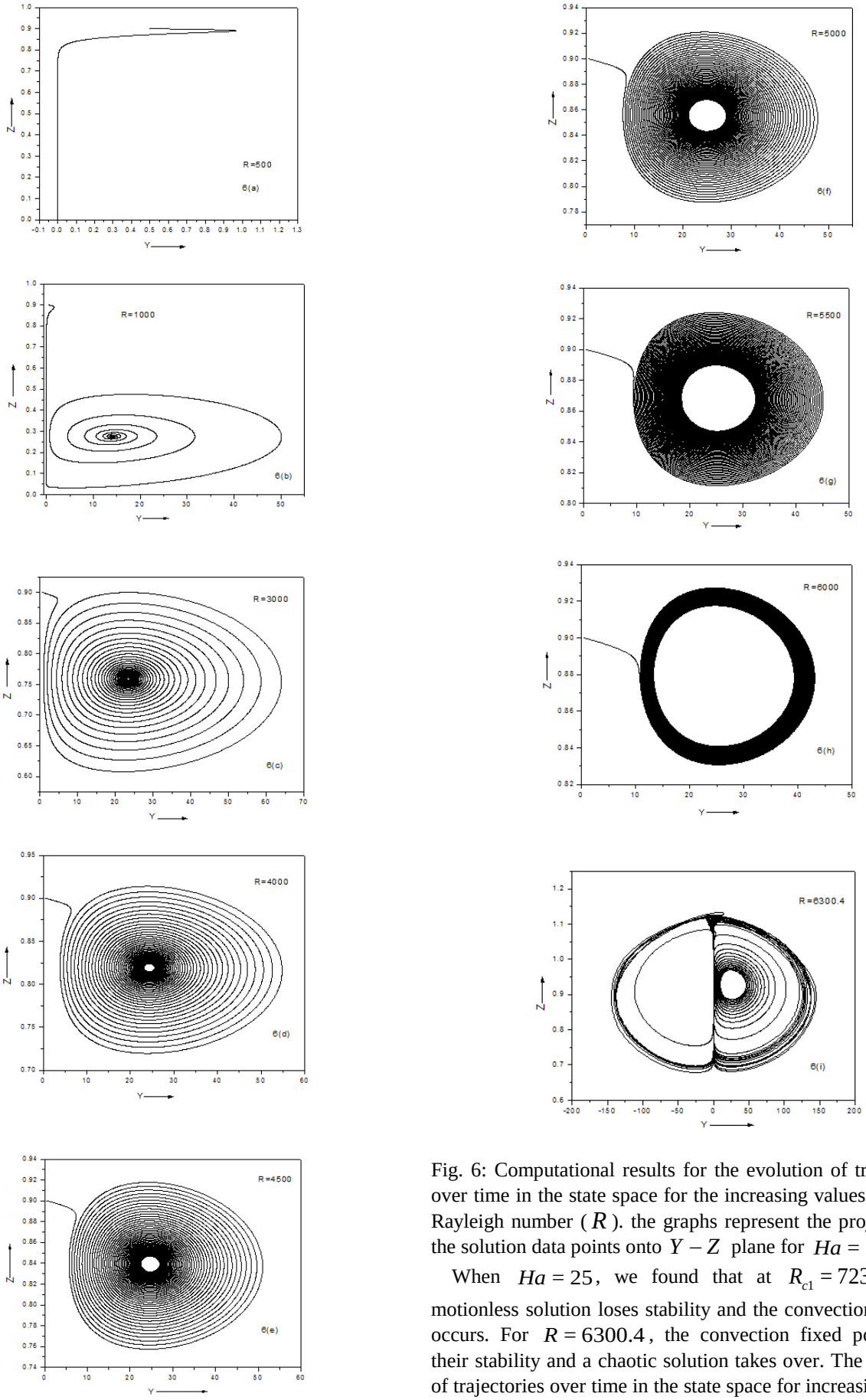

Fig. 6: Computational results for the evolution of trajectories over time in the state space for the increasing values of scaled Rayleigh number (R). the graphs represent the projection of the solution data points onto $Y-Z$ plane for $Ha = 25.$

When $Ha = 25$, we found that at $R_{c1} = 723.69$, the motionless solution loses stability and the convection solution occurs. For $R = 6300.4$, the convection fixed points lose their stability and a chaotic solution takes over. The evolution of trajectories over time in the state space for increasing values

of the scaled Rayleigh number is presented in Fig. 6 in terms of the projections of trajectories onto the $Y-Z$ plane. From Fig. $6a$, it is evident that the trajectory is like a concave curve with respect to the Y axis and moving to the steady convection point starting from initial point $(0.05,0.5,0.9)$ for $R=500$ i.e the convection solution is a stable simple node. The motionless solution losses its stability for a Rayleigh number slightly above $R_{c1}=723.69$.

In Fig. $6b$, For $R=1000$ the solutions shows that the trajectory is attracted to the convective fixed point via a spiral i.e the fixed point is a stable spiral node, which predicated a transition of the two originally real roots to a pair of complex conjugate roots at a value of $R_{c1}=723.69$.

At $R=3000$ the spiraling approach increases towards the fixed point in comparasion $R=1000$ as shown in Figs. $6c$ and $6b$ respectively. At $R=4000$, $R=4500$, $R=5000$ and $R=5500$, spiraling approach of the trajectory increases but closeness decreases towards the fixed points as shown in Fig. $6d$, $6e$, $6f$ and $6g$ respectively. Here fixed point is more stable. Fig. $6h$ shows that spiraling approach of the trajectory is maximum. It indicates that a limit cycle is created i.e. the solution is not heading anymore towards the convective fixed points but rather fluctuates periodically around it. At the value of $R=6000$, obtained solitary limit cycle indicates the loss of stability of the convection fixed points. We can observe in Fig. $6i$ that the transition to chaotic solution occurs at a critical value of $R=6300.4$.

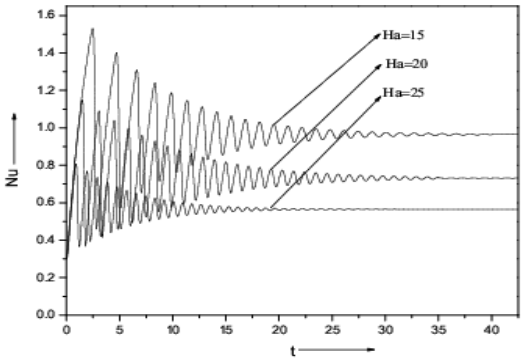

Fig. 7: Variation in Nusselt number Nu with respect to time t for values $R=1500$.

Fig. 7 shows the plots of the Nusselt number Nu with respect to time t for different values of the Hartmann number Ha. We observed that initially when t is small, the value of Nu oscillates and finally approaches to a steady state by assuming a constant value. Also, it clear that Nu approaches to its steady state at $t=20,35,40$ for $Ha=25,20,15$ respectively i.e. the convection become slower on increasing Ha. It means that the convection becomes stable with Ha.

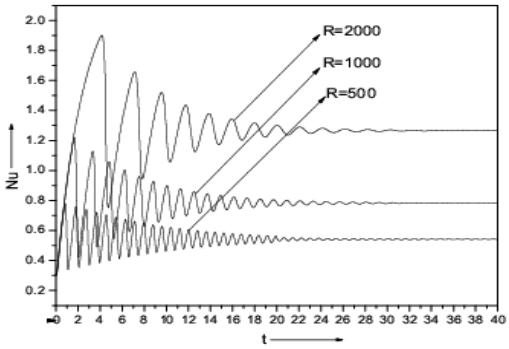

Fig. 8: Variation in Nusselt number Nu with respect to time t for $Ha=11.9$.

Fig. 8 shows the plots of Nusselt number Nu with respect to time t for $Ha=11.9$, with the variation in scaled Rayleigh number R. We observed that initially when t is small, the value of Nu oscillates and finally approaches to steady state by assuming constant value. Also, it clear that Nu approaches to its steady state at $t=28,30,32$ for $R=500,1000,2000$ respectively i.e. the convection become faster on increasing R. It means that the convection is unstable with R.

7 Conclusion

In this work, we have investigated the effect of a transverse magnetic field on chaos in a cavity subject to gravity and heated from below. Our results demonstrate different transitions, e.g. from steady convection to a non-periodic regime via a Hopf bifurcation and a further transition from chaos to periodic convection at significantly higher values of the scaled Rayleigh number. We found that there is inversely proportional relation between the Hartmann number Ha and scaled Rayleigh number R. This results provide evidence that the presence of a magnetic field delay the convection motion on chaos in a cavity i.e the system is more stable.

References

[1] M. Rucklidge, Chaos in models of double convection, Journal of Fluid Mechanics, vol. 237, pp. 209-229, 1992.
[2] S. Chandrasekhar, Hydrodynamic and Hydromagnetic Stability, (Clarendon, Oxford, 1961), Philosophical Magazine, vol. 43, pp. 146, 1952.
[3] N. O. Weiss, Numerical simulations of partial differential equation for two dimensional Boussinesq magnetoconvection and aperiodic behavior to regular oscillations. Journal of Fluid Mechanics, vol. 108, pp. 247, 1981.
[4] E. Knobloch, N. O. Weiss, and L. N. da Costa, Oscillatory and steady convection in a magnetic field. Journal of Fluid Mechanics, vol. 113, pp. 153-186, 1981.
[5] E. Knobloch and N. O. Weiss, Birfucations in a model of magnetoconvection. Physica D: Nonlinear Phenomena, vol. 9, Issue 3, pp. 379-407, 1983.
[6] E. Knobloch, D. R. Moore, J. Toomre and N. O. Weiss, Transitions to chaos in two-dimensional double-diffusive convection. Journal of Fluid Mechanics, vol. 166, pp. 409-448, 1986.
[7] Lorenz, E.N., Deterministic nonperiodic flow. Journal of the Atmospheric Sciences, vol. 20, Issue 2, pp. 130-141, 1963.

[8] A. M. Rucklidge, Chaos in a low-order model of magnetoconvection. Physica D, vol. 62, pp. 323-337, 1993.
[9] A. M. Rucklidge, Chaos in magnetoconvection. Nonlinearity, vol. 7, pp. 1565-1591, 1994.
[10] A. M. Rucklidge, N. O. Weiss, D. P. Brownjohn, P. C. Matthews, and M. R. E. Proctor, Compressible magnetoconvection in three dimensions: pattern formation in a strongly stratified layer. Journal of Fluid Mechanics, vol. 419, pp. 283-323, 2000.
[11] S. M. Cox and P. C. Matthews, New instabilities in two-dimensional rotating convection and magnetoconvection. Physica D, vol. 149, pp. 210-229, 2001.
[12] K. Matsuba, K. Imai and K. Nozaki, Nonlinear modulation of travelling rolls in magnetoconvection. Physica D, vol. 107, pp. 69-74, 1997.
[13] Chen, Z.M. and Price, W.G., On relation between Rayleigh- Benard convection and Lorenz system, Chaos Solitons Fractals, vol. 28, pp. 571-578, 2006.
[14] Bekki, N. and Moriguchi, H., Temporal chaos in Boussinesq magnetoconvection. Phys. Plasmas, vol. 14, Art. no. 012306, 2007.
[15] Garandet, J.P., Alboussiere, T. and Moreau, R., Buoyancy driven convection in a rectangular enclosure with a transverse magnetic field. International Journal of Heat and Mass Transfer, vol. 35, pp. 741–748, 1992.

NOMENCLATURE

Latin Symbols

Ar	the aspect ratio of the cavity(dimensionless),
$\bar{g}$	gravitational acceleration(m.s^{-2}), $(0,0,-g)$;
H	the height of cavity(m);
L	the length of cavity(m);
p	Pressure(N.m^{-2});
B_0	applied magnetic flux (Wb);
Ha	Hartmann number(dimensionless),
Pr	Prandtl number(dimensionless), ν/α ;
u,v	components of velocity(m.s^{-1});
Ra	Rayleigh number(dimensionless);
t	time(s);
T	temperature(K);
ΔT	temperature difference between the walls(K);

Greek symbols

κ	thermal diffusivity(m²/s);
α_T	thermal expansion coefficient(K^{-1});
μ_e	Magnetic permeability (H/m, Henry Per Meter);
ρ_0	density(Kg.m^{-3});
σ	electric conductivity (S/m, siemens per meter or);
ν	kinematic viscosity(m^2.s^{-1});
ψ	stream function(m^2.s^{-1});